

A Quark Model Calculation of $\gamma\gamma \rightarrow \pi\pi$ Including Final State Interactions

H.G. Blundell¹, S. Godfrey¹, G. Hay¹, and E.S. Swanson²

¹*Ottawa-Carleton Institute for Physics*

Department of Physics, Carleton University, Ottawa Canada K1S 5B6

²*Department of Physics and Astronomy, University of Pittsburgh,*

Pittsburgh, PA 15260 and

Jefferson Laboratory, 12000 Jefferson Ave, Newport News, VA 23606

A quark model calculation of the processes $\gamma\gamma \rightarrow \pi^+\pi^-$ and $\gamma\gamma \rightarrow \pi^0\pi^0$ is performed. At tree level, only charged pions couple to the initial state photons and neutral pions are not expected in the final state. However, a small but significant $\gamma\gamma \rightarrow \pi^0\pi^0$ cross section is observed. We demonstrate that this may be accounted for by a rotation in isospin space induced by final state interactions. The resulting $\pi^+\pi^-$ cross section is in good agreement with experiment while the $\pi^0\pi^0$ cross section is in qualitative agreement with the data.

I. INTRODUCTION

The constituent quark model has proven exceptionally successful in describing the properties of hadrons [1]. Nevertheless it is universally acknowledged that the quark model spectroscopic analysis is overly simplistic, in part because couplings of resonances to other hadronic states are not included. In particular, the quark model at its most basic level does not include final state interactions [2,3] and the effects of coupling resonances to decay channels [4]. One can view the constituent quark model as representing the lowest components of a Fock space expansion while final state interactions and coupled channel effects represent

higher order contributions. It is possible for these contributions to shift significantly the resonance pole position.

In this paper we study the contributions of final state interactions to the process $\gamma\gamma \rightarrow \pi\pi$ for relatively low center of mass energies. In this energy regime the photons have sufficiently long wavelength that they do not resolve the pions into their constituent quarks. This assertion has been formalized in the Low theorem [5], which states that scalar QED is adequate to describe $\gamma\gamma \rightarrow \pi^+\pi^-$ near threshold. However, scalar QED cannot explain the observed finite cross section to neutral pions. We will find that including final state interactions gives qualitative agreement with the data. This is nontrivial in view of the subtlety of the reaction, the expected importance of relativistic effects, and the simplifying assumptions we have made. Essentially, the $\pi^0\pi^0$ final state arises from the difference in the I=0 and I=2 $\pi\pi$ potentials which contribute to the rescattering of the final state pions in $\gamma\gamma \rightarrow \pi\pi$. Although the final state interaction contributions have been studied previously in the quark model [6], that initial study used the Fermi approximation to final state interactions, did not take into account the differences in the I=0 and I=2 potentials (which are crucial to describing the $\pi^0\pi^0$ final state), and employed rescaled pion potentials. As a result, the model of Ref. [6] predicts a substantial enhancement in charged pion production and fails when applied to neutral pion production [7]. Our conclusions differ because we have avoided these pitfalls.

Before proceeding we note that this process has been studied in other approaches which give good agreement with experiment. In particular, a recent calculation using chiral perturbation theory to two loops [8] agrees with the data as do calculations using dispersion relations with phase shift data from $\pi\pi$ scattering and constraints from unitarity, analyticity, and crossing [9]. Our purpose here is therefore not so much to explain the data but to expand the regime of applicability of the quark model and to gain some experience so that we may apply these methods to situations where the techniques just mentioned are inapplicable. Indeed, a large body of data exists on vector-vector production from $\gamma\gamma$. Much of this data is poorly understood and has led to wide spread speculation [10]. We believe that the results presented here will aid in clarifying this enigmatic situation.

We begin in section II by summarizing the scalar QED results for $\gamma\gamma \rightarrow \pi^+\pi^-$. In particular, we expand the cross section in terms of partial wave amplitudes. The expressions for the cross sections including final state interactions are derived in section III. In section IV we present our results and, finally, a summary is given in section V.

II. THE SCALAR QED CROSS SECTION FOR $\gamma\gamma \rightarrow \pi^+\pi^-$

At low energies, long wavelength photons do not probe the quark constituents of pions. Thus the pions may be rigorously treated as point particles interacting via scalar QED [5]. The cross section for the process $\gamma\gamma \rightarrow \pi^+\pi^-$ may be derived from the amplitudes shown in Fig. 1 and is given by

$$\sigma = \frac{\pi\alpha^2}{4m^2} \left[2x(1+x)\sqrt{1-x} - x^2(2-x) \ln \left(\frac{1+\sqrt{1-x}}{1-\sqrt{1-x}} \right) \right], \quad (1)$$

where $x \equiv 4m^2/s$, $s = E_{cm}^2$ is the Mandelstam variable, and m is the mass of the pion. Partial waves amplitudes, which are required when considering final state interactions, are obtained from the helicity amplitudes:

$$\begin{aligned} \mathcal{M}_{++} = \mathcal{M}_{--} &= \frac{8\pi\alpha x}{1 - (1-x)\cos^2\theta}, \\ \mathcal{M}_{\pm\mp} &= \frac{8\pi\alpha(1-x)\sin^2\theta e^{\pm 2i\phi}}{1 - (1-x)\cos^2\theta}, \end{aligned} \quad (2)$$

where θ and ϕ are the spherical polar coordinates of the outgoing π^+ and the subscripts $+$ and $-$ are the helicities of the two incoming photons. Partial wave amplitudes may be extracted as follows:

$$f_{LM_L}^{\lambda_1\lambda_2} = \int d\Omega Y_{LM_L}^*(\theta, \phi) \mathcal{M}_{\lambda_1\lambda_2}. \quad (3)$$

One finds that $f_{LM_L}^{++} = f_{LM_L}^{--}$ is only non-zero for $M_L = 0$ and that $f_{LM_L}^{+-} = f_{L-M_L}^{-+}$ is only non-zero for $M_L = 2$. The cross section is then written in terms of the partial waves as

$$\sigma = \frac{\mathcal{S}\sqrt{1-x}}{128\pi^2s} \left[(f_{00}^{++})^2 + \sum_{L \geq 2, \text{even}}^{\infty} [(f_{L0}^{++})^2 + (f_{L2}^{+-})^2] \right] \quad (4)$$

where $\mathcal{S} \equiv 1/(1 + \delta_{\pi\pi})$ is a statistical factor required for the $\pi^0\pi^0$ channel (to be discussed below). The necessary partial waves are given by:

$$\begin{aligned}
f_{00}^{+++} &= 8\pi^{\frac{3}{2}}\alpha \frac{x}{\sqrt{1-x}} \ln\left(\frac{1+\sqrt{1-x}}{1-\sqrt{1-x}}\right), \\
f_{20}^{+++} &= 4\sqrt{5}\pi^{\frac{3}{2}}\alpha \frac{x}{1-x} \left[-6 + \frac{2+x}{\sqrt{1-x}} \ln\left(\frac{1+\sqrt{1-x}}{1-\sqrt{1-x}}\right)\right], \\
f_{22}^{+-} &= 4\sqrt{\frac{15}{2}}\pi^{\frac{3}{2}}\alpha \left[\frac{10}{3} - \frac{2}{1-x} + \frac{x^2}{(1-x)^{\frac{3}{2}}} \ln\left(\frac{1+\sqrt{1-x}}{1-\sqrt{1-x}}\right)\right], \\
f_{40}^{+++} &= 3\pi^{\frac{3}{2}}\alpha \frac{x}{1-x} \left[\frac{110}{3} - \frac{70}{1-x} + \frac{3x^2+24x+8}{(1-x)^{\frac{3}{2}}} \ln\left(\frac{1+\sqrt{1-x}}{1-\sqrt{1-x}}\right)\right], \\
f_{42}^{+-} &= 3\sqrt{10}\pi^{\frac{3}{2}}\alpha \left[\frac{-54}{5} + \frac{76}{3(1-x)} - \frac{14}{(1-x)^2} + \frac{x^2(6+x)}{(1-x)^{\frac{5}{2}}} \ln\left(\frac{1+\sqrt{1-x}}{1-\sqrt{1-x}}\right)\right], \\
f_{60}^{+++} &= 8\sqrt{13}\pi^{\frac{3}{2}}\alpha \frac{x}{1-x} \left[-\frac{231}{40} + \frac{7(4-15x)}{8(1-x)} - \frac{21(1+5x+5x^2)}{8(1-x)^2} \right. \\
&\quad \left. + \frac{16+120x+90x^2+5x^3}{16(1-x)^{\frac{5}{2}}} \ln\left(\frac{1+\sqrt{1-x}}{1-\sqrt{1-x}}\right)\right]. \tag{5}
\end{aligned}$$

III. FINAL STATE INTERACTIONS

Final state interactions (FSI) are additional interactions between particles in the final state that are not included in the basic interaction. In our problem the basic interaction is the scalar QED process described in the previous section and the FSI's are purely hadronic and are described by effective potentials between the outgoing particles. We use the distorted wave Born approximation in our calculations [3], which relies on nonrelativistic quantum mechanics. We include relativistic phase space where possible and use the relativistic scalar QED result for the basic interaction. This mixture of nonrelativistic and relativistic elements is typical of the quark model.

The first step in including FSI's is to find the wavefunction describing the relative motion of the final-state particles due to the FSI potentials alone. We choose to do this by solving a two body Schrödinger equation with an effective $\pi\pi$ interaction. The scattered waves are written in terms of spherical waves as

$$\psi_{\vec{k}}^{-}(\vec{r}) = 4\pi \sum_{l=0}^{\infty} \sum_{m_l=-l}^l i^l e^{-i\delta_l} u_l(k, r) Y_{lm_l}^*(\Omega_k) Y_{lm_l}(\Omega_r) \quad (6)$$

where $u_l(k, r)$, the radial solution of the Schrödinger equation, has the asymptotic form

$$u_l(k, r) \xrightarrow{r \rightarrow \infty} \frac{1}{kr} \sin(kr - \frac{1}{2}l\pi + \delta_l). \quad (7)$$

Here k is the relative momentum between the particles, $k^2 = 2\mu E$, where μ is the reduced mass of the particles and E is the total energy of the system.

The $\pi\pi$ potentials used to derive the final state wavefunction are taken from Refs. [11,12]. These are obtained by calculating the perturbative T-matrix for a given process in the nonrelativistic quark model. This T-matrix was then equated to a model pointlike T-matrix to obtain an effective interaction. The quark model calculation includes one gluon exchange and confinement interactions followed by quark rearrangement into final state color singlets. For the I=0 channel there is an additional contribution from $q\bar{q}$ annihilation. The resulting effective potentials are parametrized in the form

$$V_{\pi\pi}(r) = V_0 e^{-\frac{1}{2}\left(\frac{r}{r_0}\right)^2}. \quad (8)$$

The parameters, V_0 and r_0 , are reproduced in Table 1. FSI corrections were only made to the S-wave amplitudes because corrections to D-waves were found to have a negligible effect on the cross section.

Final state interactions are incorporated with the standard two-potential relation [2,3]:

$$\langle f|T|i \rangle^{\text{FSI}} = \langle \psi_{\vec{k}_f}^{-} | W | \phi_{\vec{k}_i} \rangle = \frac{1}{(2\pi)^{\frac{3}{2}}} \int d^3\vec{k} \psi_{\vec{k}_f}^{-*}(\vec{k}) \langle f|T|i \rangle \quad (9)$$

where $\psi_{\vec{k}_f}^{-*}(\vec{k})$ is the complex conjugate of the momentum-space solution of the Schrödinger equation with the FSI potential $V_{\pi\pi}$, W is the basic electromagnetic interaction, and $\phi_{\vec{k}}$ is a plane wave. The corrected QED amplitude is

$$\begin{aligned} \mathcal{M}^{\text{FSI}}(\vec{k}_f) &= \frac{2}{\pi} \sqrt{s(k_f)} \sum_{l=0}^{\infty} \sum_{m_l=-l}^l e^{i\delta_l} Y_{lm_l}(\Omega_{k_f}) \\ &\times \int d^3\vec{k} \frac{\mathcal{M}(\vec{k})}{\sqrt{s(k)}} Y_{lm_l}^*(\Omega_k) \int_0^{\infty} dr r^2 j_l(kr) u_l(k_f, r) \end{aligned}$$

where $\mathcal{M}(\vec{k})$ is the uncorrected scalar QED amplitude, $j_l(kr)$ is a spherical Bessel function and the \sqrt{s} factors are introduced to relate the relativistic QED amplitudes to the nonrelativistic amplitudes used in the calculation.

In order to include the FSI correction for each partial wave we decompose the amplitudes

$$\mathcal{M}^{FSI}(\vec{k}) \equiv \sum_{L=0}^{\infty} \sum_{M_L=-L}^L f_{LM_L}^{FSI}(s(k)), Y_{LM_L}(\Omega_k) \quad (10)$$

where the corrected partial wave amplitudes are given by

$$f_{LM_L}^{FSI}(s(k_f)) = \frac{2}{\pi} \sqrt{s(k_f)} e^{i\delta_L} \int_0^\infty dk \int_0^\infty dr r^2 k^2 \frac{f_{LM_L}(s(k))}{\sqrt{s(k)}} j_L(kr) u_L(k_f, r). \quad (11)$$

Helicity labels have been omitted. In the absence of an FSI potential, $\delta_L \rightarrow 0$ and $u_L(k_f, r) \rightarrow j_L(k_f r)$, the orthogonality of the spherical Bessel functions yields a delta function, and we recover $f_{LM_L}^{FSI}(s(k_f)) \rightarrow f_{LM_L}(s(k_f))$ as expected.

The relationship between the charged pion basis of the physical scalar QED reaction and the isospin basis of the potentials is

$$\begin{aligned} |\pi^+\pi^-\rangle &= \sqrt{\frac{2}{3}} |00\rangle + \sqrt{\frac{1}{3}} |20\rangle, \\ |\pi^0\pi^0\rangle &= -\sqrt{\frac{1}{3}} |00\rangle + \sqrt{\frac{2}{3}} |20\rangle. \end{aligned}$$

Thus, the physical pion wavefunctions can be written in terms of the momentum space solutions of the Schrödinger equation in the isospin basis:

$$\begin{aligned} \psi^{-\pi^+\pi^-*}(k) &= \langle \psi_{\vec{k}_f}^{-\pi^+\pi^-} | \phi_{\vec{k}}^{\pi^+\pi^-} \rangle = \left[\sqrt{\frac{2}{3}} \langle \psi_{\vec{k}_f}^{-0} | + \sqrt{\frac{1}{3}} \langle \psi_{\vec{k}_f}^{-2} | \right] \left[\sqrt{\frac{2}{3}} |\phi_{\vec{k}}^0\rangle + \sqrt{\frac{1}{3}} |\phi_{\vec{k}}^2\rangle \right] \\ &= (2\pi)^{\frac{3}{2}} \left[\frac{2}{3} \psi_{\vec{k}_f}^{-0*}(\vec{k}) + \frac{1}{3} \psi_{\vec{k}_f}^{-2*}(\vec{k}) \right], \\ \psi^{-\pi^0\pi^0*} &= \langle \psi_{\vec{k}_f}^{-\pi^0\pi^0} | \phi_{\vec{k}}^{\pi^+\pi^-} \rangle = (2\pi)^{\frac{3}{2}} \left[-\frac{\sqrt{2}}{3} \psi_{\vec{k}_f}^{-0*}(\vec{k}) + \frac{\sqrt{2}}{3} \psi_{\vec{k}_f}^{-2*}(\vec{k}) \right]. \end{aligned}$$

The corrected partial waves for $\pi^+\pi^-$ production are thus given by

$$\begin{aligned} f_{LM_L}^{FSI}{}_{\pi^+\pi^-}(s(k_f)) &= \frac{2}{\pi} \sqrt{s(k_f)} \int_0^\infty dk \int_0^\infty dr r^2 k^2 \frac{f_{LM_L}(s(k))}{\sqrt{s(k)}} \\ &\times j_L(kr) \left[\frac{2}{3} e^{i\delta_L^0} u_L^0(k_f, r) + \frac{1}{3} e^{i\delta_L^2} u_L^2(k_f, r) \right] \quad (12) \end{aligned}$$

with an analogous expression for the $\pi^0\pi^0$ final state. Here δ_L^I is the $\pi\pi$ phase shift in the isospin I , partial wave L channel. To simplify the following expressions we define the isospin amplitudes

$$g_{LM_L}^I(s(k_f)) \equiv \frac{2}{\pi} \sqrt{s(k_f)} \int_0^\infty dk \int_0^\infty dr r^2 k^2 \frac{f_{LM_L}(s(k))}{\sqrt{s(k)}} j_L(kr) u_L^I(k_f, r). \quad (13)$$

This yields the final state enhanced probability for $\pi^+\pi^-$ production:

$$|f_{LM_L}^{\text{FSI } \pi^+\pi^-}|^2 = \frac{4}{9} (g_{LM_L}^0)^2 + \frac{1}{9} (g_{LM_L}^2)^2 + \frac{4}{9} g_{LM_L}^0 g_{LM_L}^2 \cos(\delta_L^0 - \delta_L^2) \quad (14)$$

and for $\pi^0\pi^0$ production:

$$|f_{LM_L}^{\text{FSI } \pi^0\pi^0}|^2 = \frac{2}{9} (g_{LM_L}^0)^2 + \frac{2}{9} (g_{LM_L}^2)^2 - \frac{4}{9} g_{LM_L}^0 g_{LM_L}^2 \cos(\delta_L^0 - \delta_L^2). \quad (15)$$

With no $\pi\pi$ potentials $g_{LM_L} \rightarrow f_{LM_L}$ and $\delta_L^I = 0$ and the original cross sections are recovered.

The last step is to account for the limited polar acceptance of the $\pi\pi$ experimental data. Integrating over a finite solid angle ($-\cos\theta_{\text{acc}} \leq \cos\theta \leq \cos\theta_{\text{acc}}$) to obtain the uncorrected cross section for limited polar acceptance is straightforward: Eq. 1 is replaced by

$$\sigma_{\text{acc}} = \frac{\pi\alpha^2}{4m^2} \left[2 \cos\theta_{\text{acc}} x \sqrt{1-x} \left(\frac{x^2}{1 - (1-x) \cos^2\theta_{\text{acc}}} + 1 \right) - x^2(2-x) \ln \left(\frac{1 + \sqrt{1-x} \cos\theta_{\text{acc}}}{1 - \sqrt{1-x} \cos\theta_{\text{acc}}} \right) \right]. \quad (16)$$

However, the expression in terms of partial waves is affected more drastically as the spherical harmonics are no longer orthogonal to each other and the contributions of the partial waves to the total cross section can no longer be separated. The expression replacing Eq. 4 becomes an infinite sum.

$$\sigma_{\text{acc}} = \frac{\sqrt{1-x}}{256\pi^2 s} \int_0^{2\pi} d\phi \int_{-\cos\theta_{\text{acc}}}^{\cos\theta_{\text{acc}}} d(\cos\theta) \left[2 \left| \sum_{L \geq 0, \text{even}}^\infty f_{L0} Y_{L0}(\theta, \phi) \right|^2 + \left| \sum_{L \geq 2, \text{even}}^\infty f_{L2} Y_{L2}(\theta, \phi) \right|^2 + \left| \sum_{L \geq 2, \text{even}}^\infty f_{L2} Y_{L-2}(\theta, \phi) \right|^2 \right]. \quad (17)$$

Because the $L = 0$ partial wave is the only one affected significantly by FSI's, we assume that all of the observed $\gamma\gamma \rightarrow \pi^0\pi^0$ events are in an $L = 0$ state. Since that distribution is

spherically symmetric, we can correct the data by simply dividing by the value of $\cos \theta_{\text{acc}}$ appropriate to the experiment in question.

For $\gamma\gamma \rightarrow \pi^+\pi^-$ the total observed cross section is a mixture of all partial waves. We again assume that only the $L = 0$ wave is affected by FSI's. To simplify our calculations we define the harmonic integrals

$$h_{l_1 l_2}^m \equiv \int_0^{2\pi} d\phi \int_{-\cos \theta_{\text{acc}}}^{\cos \theta_{\text{acc}}} d(\cos \theta) Y_{l_1 m}^*(\theta, \phi) Y_{l_2 m}(\theta, \phi) \quad (18)$$

and note that $h_{l_1 l_2}^m = h_{l_2 l_1}^m$ and $h_{l_1 l_2}^{-2} = h_{l_1 l_2}^2$ (h is independent of m). We can then write the total cross section with only the $L = 0$ partial wave corrected for FSI's as the total uncorrected cross section, plus an infinite number of correction terms, each of which is the difference between the corrected and uncorrected values of a term in Eq. 17. Only those terms involving f_{00} , which goes to $f_{00}^{\text{FSI}}_{\pi^+\pi^-}$, need correcting. Eq. 4 is replaced by

$$\begin{aligned} \sigma_{\text{acc}, \pi^+\pi^-}^{\text{FSI}} &= \sigma_{\text{acc}} + \frac{\sqrt{1-x}}{128\pi^2 s} \left[h_{00}^0 \left\{ |f_{00}^{\text{FSI}}_{\pi^+\pi^-}|^2 - (f_{00})^2 \right\} \right. \\ &\quad \left. + \sum_{L \geq 2, \text{even}}^{\infty} h_{L0}^0 \left\{ f_{00}^{\text{FSI}}_{\pi^+\pi^-} f_{L0} + (f_{00}^{\text{FSI}}_{\pi^+\pi^-})^* f_{L0} - 2f_{00} f_{L0} \right\} \right] \\ &= \sigma_{\text{acc}} + \frac{\sqrt{1-x}}{128\pi^2 s} \left[h_{00}^0 \left\{ \frac{4}{9} (g_{00}^0)^2 + \frac{1}{9} (g_{00}^2)^2 + \frac{4}{9} g_{00}^0 g_{00}^2 \cos(\delta_0^0 - \delta_0^2) - (f_{00})^2 \right\} \right. \\ &\quad \left. + \sum_{L \geq 2, \text{even}}^{\infty} 2 h_{L0}^0 f_{L0} \left\{ \frac{2}{3} g_{00}^0 \cos \delta_0^0 + \frac{1}{3} g_{00}^2 \cos \delta_0^2 - f_{00} \right\} \right]. \quad (19) \end{aligned}$$

Excellent convergence over the relevant energy range is obtained when the series is truncated after $L = 6$. Fortunately, the three experiments whose data we use for comparisons all have the same limited polar acceptance ($|\cos \theta| \leq 0.6$), so the results need be corrected for only one value of $\cos \theta_{\text{acc}}$.

IV. RESULTS

Equation (13) demonstrates that the isospin dependence of the $\pi\pi$ production amplitudes is generated through the isospin dependence of the final state interactions. The fact that

the isoscalar and isotensor $\pi\pi$ interactions differ markedly causes a rotation in isospin space which is reflected in a nonzero $\pi^0\pi^0$ amplitude (see Equation (15)). Indeed, strong, but isospin independent, $\pi\pi$ interactions would *not* give rise to neutral pions in the final state.

Equation (15) reveals that the details of the neutral pion prediction depend on the scalar QED production mechanism, the isoscalar and isotensor hadronic phase shifts, and FSI-induced modifications to the outgoing pion-pion wavefunction. We shall assume that the tree order scalar QED amplitude captures most of the production mechanism (we note that direct $\gamma\gamma$ coupling to the f_0 and rescattering to $\pi^0\pi^0$ is possible – this is discussed below) and that the joining of relativistic and nonrelativistic formalisms has not overly distorted the predictions.

The S-wave elastic phase shifts produced by the $\pi\pi$ potentials are shown as solid lines in Figures 3 ($I = 2$) and 4 ($I = 0$). It is clear that both underestimate the strength of the $\pi\pi$ interaction. However, it has been shown [17] that the majority of this discrepancy may be alleviated by employing relativistic kinematics in the description of the $\pi\pi$ phase shift. This yields the dashed curves in Figures 3 and 4. The agreement in the isotensor sector is quite good. The isoscalar prediction is still somewhat low; however, the isoscalar sector differs from the isotensor sector in that $q\bar{q}$ annihilation will lead to resonance coupling. Indeed, the authors of Ref. [11] have shown that very good agreement may be achieved once the neglected effects of mixing with the $f_0(980)$ and $f_0(1350)$ are included. Since resonance coupling will also induce wavefunction effects in our problem, we have chosen to examine the importance of the phase shifts by simply fitting them. The fits are indicated as dotted lines in Figures 3 and 4. The differences between the predictions for neutral pion production for the relativized model (dashed lines) and the fits (dotted lines) will be examined below.

The final contribution to the $\pi^0\pi^0$ cross section came from the FSI-induced distortions to the pion-pion wavefunction. We shall assume that this is accurately described by our potential formalism. This may appear doubtful because the potential phase shifts did not agree well with elastic $\pi\pi$ scattering data. However, as noted above, the majority of the discrepancy is due to the nonrelativistic phase space necessitated by the numerical solution

of the Schrödinger equation, rather than the potential itself. We are thus confident that the effective potentials can describe the wavefunction distortion. However, the model neglects additional distortions to the wavefunction caused by transitions to virtual resonance states (the f_0). For the moment, we will assume that these are small near threshold since the $f_0(980)$ is narrow and the $f_0(1350)$ is distant. Indeed, calculations with a relativistic Breit-Wigner yield the following cross sections for $\pi^0\pi^0$ at threshold: 0.015 nb for $f_0(980)$, 0.00005 nb for $f_0(1275)$, and 0.15 nb for $f_2(1275)$.

Figure 5b shows the predicted cross section for $\gamma\gamma \rightarrow \pi^+\pi^-$ along with data from three experiments. There is very little difference between predictions, indicating the lack of importance of FSI effects in the charged channel. The Born result agrees fairly well with the data. The Born result also agrees well with the dispersion analysis of Ref. [9] for $\sqrt{s} < 350$ MeV, where there is no data.

The dashed line of Figure 5a is the predicted cross section for $\pi^0\pi^0$ production which is based on the relativized $\pi\pi$ phase shift predictions of Ref. [12] and a nonrelativistic $\pi\pi$ final state wavefunction. Recall that this curve therefore does not incorporate resonance effects and does not fit the isoscalar $\pi\pi$ scattering data well. The result presented in Figure 5a agrees well with data near threshold – an indication that the near threshold neutral pion data can be explained by the postulated mechanism of final state interaction-induced isospin rotation. Nevertheless, the dashed curve falls below the data by a factor of three or four above energies of 350 MeV. It is therefore of interest to test the effects of intermediate resonance states. We model this by fitting the experimental S-wave $\pi\pi$ phase shifts as described above. Note that we are ignoring wavefunction distortion caused by dynamical resonance effects. The resulting prediction is given by the dotted line in Figure 5a. The agreement with data is substantially improved. This is due to the increased accuracy of the description of the $I = 0$ scattering data and is a strong indication that resonance effects (as manifested in the $I = 0$ phase shift) can be important even near threshold.

The agreement with experiment is not perfect – we believe that this is likely due to explicit dynamical resonance effects in the final state scattering wavefunction. It should be

possible to test this assertion by including resonances in a coupled channel description of the final state interactions. Nevertheless, the main point is established – it is possible to describe the rather complicated processes leading to a $\pi^0\pi^0$ final state with a sufficiently detailed analysis of the production mechanism and the final state interactions.

V. CONCLUSIONS

The reaction $\gamma\gamma \rightarrow \pi^0\pi^0$ presents an interesting theoretical challenge. Neutral pions do not couple directly to low energy photons so that direct techniques based on the Low theorem cannot be used to describe the cross section. Calculations tend to be difficult; this is illustrated by efforts in chiral perturbation theory which have found it necessary to introduce three new counterterms, work to two loops, and to unitarize. We have presented a relatively simple explanation of the data. In our model neutral pion production proceeds via charged pion production followed by final state hadronic interactions. The $\pi^+\pi^-$ initial state is described well by the Born order scalar QED amplitude, in accord with Low’s theorem. This amplitude is then convoluted with the final state pion-pion wavefunction to arrive at a prediction for $\pi^0\pi^0$ production.

The result for $\gamma\gamma \rightarrow \pi^+\pi^-$ is very insensitive to final state interactions – a result that follows from isospin algebra and the weakness of the final state interactions [28]. However, the prediction for $\pi^0\pi^0$ depends crucially on the interference between $I = 0$ and $I = 2$ final state interactions, and is therefore driven by the well known differences in these processes – $I = 2$ S-wave $\pi\pi$ scattering is repulsive while $I = 0$ is attractive. It was shown in Ref. [11] that roughly half of the scattering strength at low energy in $I = 0$ is due to the $f_0(980)$ and $f_0(1350)$ resonances – even at threshold. This leads to the surprising conclusion that resonance coupling is important to getting the magnitude of the $\pi^0\pi^0$ cross section correct near threshold.

This calculation was undertaken with an eye to extensions to heavier systems. In particular, $\gamma\gamma$ production of vector-vector states has a long, and enigmatic, history. For example,

the large ratio $\sigma(\gamma\gamma \rightarrow \rho^0\rho^0)/\sigma(\gamma\gamma \rightarrow \rho^+\rho^-)$ is problematic and has engendered much speculation. This is due, in part, to the lack of clear theoretical guidance – chiral perturbation theory and dispersion methods are inapplicable for these processes. Of course such constraints do not exist on the quark model and we look forward to applying it to an explication of this interesting area of hadronic physics.

ACKNOWLEDGMENTS

The authors are grateful to Ted Barnes for extensive discussions on $\gamma\gamma$ physics. This research was supported in part by the Natural Sciences and Engineering Research Council of Canada and by the United States Department of Energy under grant DE-FG02-96ER40944 and contract DE-AC05-84ER40150 under which the Southeastern Universities Association operates the Thomas Jefferson National Accelerator Facility.

REFERENCES

- [1] See for example S. Godfrey, *Nuovo Cim.* **102A**, 1 (1989); S. Godfrey and N. Isgur, *Phys. Rev. D* **32**, 189 (1985); S. Capstick and N. Isgur, *Phys. Rev. D* **34**, 2809 (1986).
- [2] See for example John Gillespie, *Final-State Interactions* (Holden-Day, San Francisco, 1964).
- [3] Albert Messiah, *Quantum Mechanics*, translated from the French by G.M. Temmer (vol. 1) and J. Potter (vol. 2) (John Wiley & Sons, New York, 1961-5).
- [4] N. Tornqvist, *Annals of Physics*, **123**, 1 (1979); John Weinstein, “The Multichannel Quark Model”, Preprint UMHEP 96-021, University of Mississippi, nucl-th/9606037, (1996); E.S. Swanson, “Final State Interactions”, *Proceedings from CMU/JLab Workshop on Physics with 8+ GeV Photons*, ed. C. Meyer, (JLab, Newport News, 1998).
- [5] F.E. Low, *Phys. Rev.* **96**, 1428 (1954).
- [6] T. Barnes, K. Dooley, and N. Isgur, *Phys. Lett.* **B183**, 210 (1987).
- [7] M.R. Pennington, *Two Photons in: Two Pions Out*, Proc. Workshop on Physics and Detectors at Daphne, Frascati, 1991. Ed. G. Pancheri.
- [8] S. Bellucci, J. Gasser, and M.E. Sainio, *Nucl. Phys. B* **423**, 80 (1994); Erratum **431**, 413 (1994).
- [9] D. Morgan and M.R. Pennington, *Phys. Lett.* **272B**, 134 (1991); **192B**, 207 (1987); J.F. Donoghue and B.R. Holstein, *Phys. Rev.* **D48**, 137 (1993).
- [10] Bing An Li and K.F. Liu, *Phys. Lett.* **118B**, 435 (1982); Erratum, *Phys. Lett.* **124B**, 550 (1983); N.N. Achasov, S.A. Devyanin, and G.N. Shestakov, *JETP Lett.* **40**, 1173 (1984).
- [11] Z. Li, M. Guidry, T. Barnes, and E.S. Swanson, [hep-ph/9401326] (1994).
- [12] T. Barnes and E.S. Swanson, *Phys. Rev.* **D46**, 131(1991).

- [13] W. Hoogland *et al.*, Nucl. Phys. B **126**, 109 (1977).
- [14] J.P. Prukop *et al.*, Phys. Rev. D **10**, 2055 (1974).
- [15] Durham/RAL HEP Reaction Data Database at <http://durpdg.dur.ac.uk/HEPDATA>.
- [16] D. Morgan, M.R. Pennington, and M.R. Whalley, J. Phys. G **20**, A1 (1994).
- [17] E.S. Swanson, Ann. Phys. (N.Y.) **220**, 73 (1992).
- [18] K.N. Mukhin *et al.*, Pis' ma Zh. Eksp. Teor. Fiz. **32**, 616 (1980) [JETP Lett. **32**, 601 (1980)].
- [19] L. Rosselet *et al.*, Phys. Rev. D **15**, 574 (1977).
- [20] P. Estabrooks and A.D. Martin, Nucl. Phys. B **79**, 301 (1974).
- [21] S.D. Protopopescu *et al.*, Phys. Rev. D **7**, 1279 (1973).
- [22] Crystal Ball Collaboration (J.K. Bienlein for the collaboration), Proceedings of the IX International Workshop on Photon-Photon Collisions, ed. by D. Caldwell and H.P. Paar (World Scientific, Singapore, 1992), p. 241.
- [23] Crystal Ball Collaboration, H. Marsiske *et al.*, Phys. Rev. **D41**, 3324 (1990).
- [24] C. Edwards *et al.*, Phys. Lett. **B110**, 82 (1982).
- [25] CELLO Collaboration, H.J. Behrend *et al.*, Z. Phys **C56**, 381 (1992).
- [26] J. Boyer *et al.*, Phys. Rev. **D42**, 1350 (1990).
- [27] TPC/Two Gamma Collaboration, H. Aihara *et al.*, Phys. Rev. Lett. **57**, 404 (1986).
- [28] E.S. Swanson, Nuovo Cim. **107A**, 2367 (1994).

FIGURES

FIG. 1. The tree-level Feynman diagrams for the scalar QED contributions to $\gamma\gamma \rightarrow \pi^+\pi^-$. The labels denote the particle momenta (p_i) and photon polarizations (ϵ_i).

FIG. 2. The $\pi\pi$ potentials vs r for $I = 0, L = 0$ (solid line), $I = 0, L = 2$ (dashed line), $I = 2, L = 0$ (dotted line), and $I = 2, L = 2$ (dot-dot-dashed line). The potentials are given by Eqn. 8 with the parameters given in Table I.

FIG. 3. The $I = 2$ $\pi\pi$ scattering phase shift vs. \sqrt{s} using $\pi\pi$ potentials (solid line), the quark model prediction [11] (dashed line), and a linear approximation to the experimental data, $\delta_{L=0}^{I=2} = -0.00062 \text{ rad/MeV} \times (\sqrt{s} - 250 \text{ MeV})$ (dotted line). The data are from Hoogland *et al.* (circles) [13] – we show the results of both of their methods; and Prukop *et al.* (triangles) [14] – we show the results of their first fit. Some of the data shown in this figure were obtained from References [15] and [16]. The horizontal error bars on the data indicate bin size; for the vertical error bars all of the given errors were added in quadrature.

FIG. 4. The $I = 0$ $\pi\pi$ scattering phase shift vs. \sqrt{s} , using $\pi\pi$ potentials (solid line), the quark model prediction without resonance contributions (see text) [11] (dashed line), and a linear approximation to the experimental data, $\delta_{L=0}^{I=0} = 0.0027 \text{ rad/MeV} \times (\sqrt{s} - 250 \text{ MeV})$ (dotted line). The data are from Mukhin *et al.* (circles) [18]; Rosselet *et al.* (inverted triangles) [19] – the horizontal bars only approximate their bins, and their data is actually for $\delta_0^0 - \delta_1^1$ – we have used the δ_0^0 data extracted from it by Li *et al.* [11]; Estabrooks and Martin [20] – we show the results of both their s- (squares) and t-channel fits (diamonds); and Protopopescu *et al.* (triangles) [21] – we show the results of their case 1. For further comments see Fig. 3.

FIG. 5. (a) $\sigma(\gamma\gamma \rightarrow \pi^0\pi^0)$ vs \sqrt{s} , using phase shifts from the quark model (dashed line), from linear fits to the data (dotted line), and experimental data. The data are from Bienlein (*et al.*) (closed circles) [22], Marsiske *et al.* (open circles) [23] and Edwards *et al.* (closed triangles) [24]. The data have been corrected to full polar acceptance, $|\cos\theta| \leq 1.0$. (b) $\sigma(\gamma\gamma \rightarrow \pi^+\pi^-)$ vs. \sqrt{s} with the same line labelling as (a). The curves have been corrected to have a limited polar acceptance to match the data: $|\cos\theta| \leq 0.6$. The data are from Behrend *et al.* (closed circles) [25], Boyer *et al.* (open circles) [26], and Aihara *et al.* (closed triangles) [27]. For additional comments see Figure 3.

Table 1: The parameters of the $\pi - \pi$ potentials used in this work [17,11]. The t-channel gluon exchange potentials have two contributions, due to colour-hyperfine and confinement terms, which must be summed. The potentials use the parametrization of Eqn. 8 with V_0 in GeV, r_0 in GeV^{-1} .

Pion State		t-channel gluon exchange				s-channel	
L	I	hyperfine		confinement		gluon exchange	
		V_0	r_0	V_0	r_0	V_0	r_0
0	0	-0.392	1.36	-0.024	2.29	-1.75	1.48
0	2	0.786	1.36	0.047	2.29		
2	0	-0.044	1.40	0.0175	1.49		
2	2	0.088	1.40	-0.035	1.49		

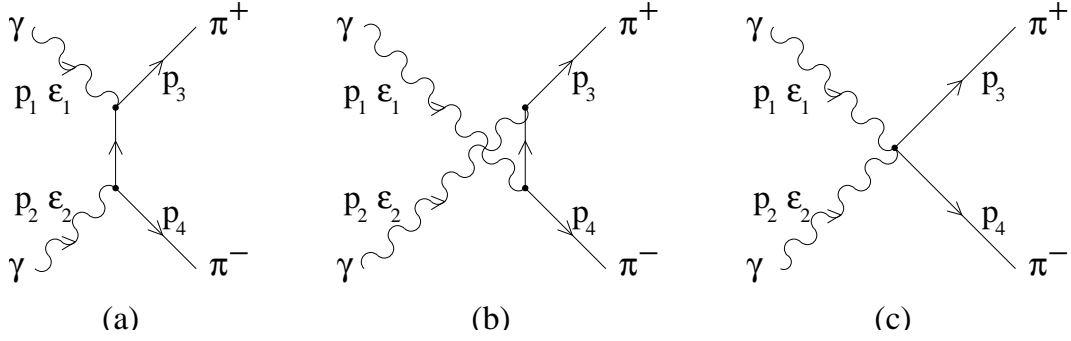


Fig 1: The tree-level Feynman diagrams for the scalar QED contributions to $\gamma\gamma \rightarrow \pi^+\pi^-$. The labels denote the particle momenta (p_i) and photon polarizations (ϵ_i).

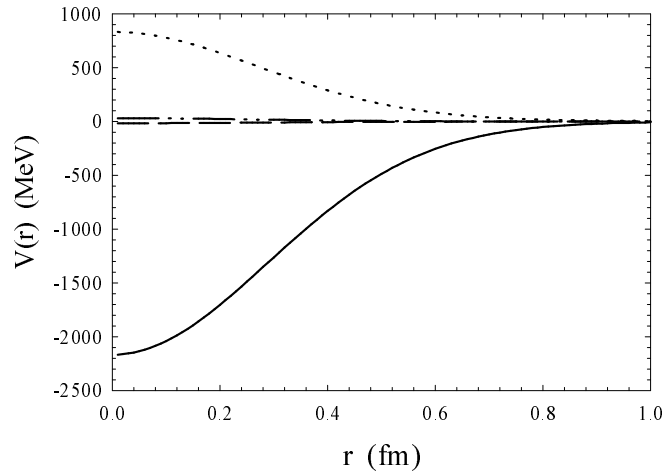


Fig 2: The $\pi\pi$ potentials vs r for $I = 0, L = 0$ (solid line), $I = 0, L = 2$ (dashed line), $I = 2, L = 0$ (dotted line), and $I = 2, L = 2$ (dot-dot-dashed line). The potentials are given by Eqn. 8 with the parameters given in Table I.

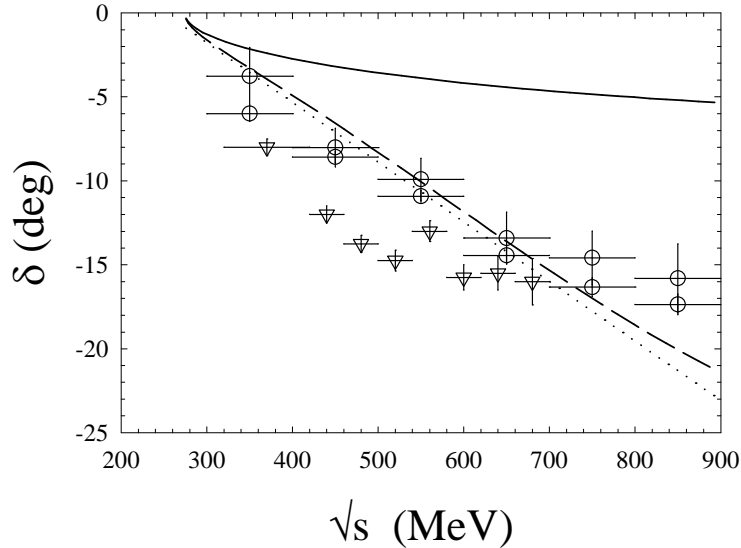


Figure 3: The $I = 2$ $\pi\pi$ scattering phase shift vs. \sqrt{s} using $\pi\pi$ potentials (solid line), the quark model prediction [11] (dashed line), and a linear approximation to the experimental data, $\delta_{L=0}^{I=2} = -0.00062 \text{ rad/MeV} \times (\sqrt{s} - 250 \text{ MeV})$ (dotted line). The data are from Hoogland *et al.* (circles) [13] – we show the results of both of their methods; and Prukop *et al.* (triangles) [14] – we show the results of their first fit. Some of the data shown in this figure were obtained from References [15] and [16]. The horizontal error bars on the data indicate bin size; for the vertical error bars all of the given errors were added in quadrature.

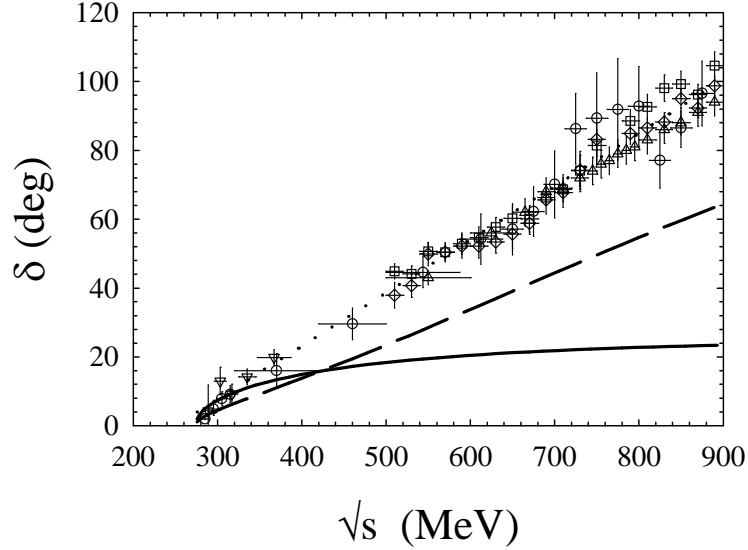


Figure 4: The $I = 0$ $\pi\text{-}\pi$ scattering phase shift vs. \sqrt{s} , using $\pi\pi$ potentials (solid line), the quark model prediction without resonance contributions (see text) [11] (dashed line), and a linear approximation to the experimental data, $\delta_{L=0}^{I=0} = 0.0027 \text{ rad/MeV} \times (\sqrt{s} - 250 \text{ MeV})$ (dotted line). The data are from Mukhin *et al.* (circles) [18]; Rosselet *et al.* (inverted triangles) [19] – the horizontal bars only approximate their bins, and their data is actually for $\delta_0^0 - \delta_1^1$ – we have used the δ_0^0 data extracted from it by Li *et al.* [11]; Estabrooks and Martin [20] – we show the results of both their s- (squares) and t-channel fits (diamonds); and Protopopescu *et al.* (triangles) [21] – we show the results of their case 1. For further comments see Fig. 3.

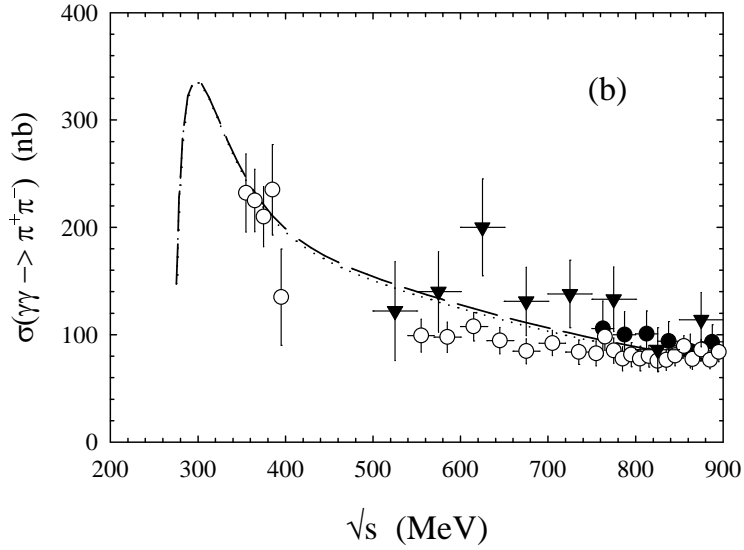
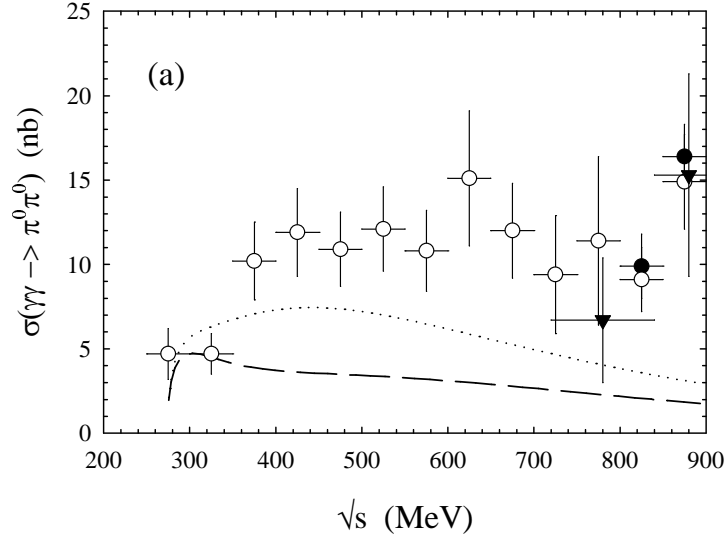


Figure 5: (a) $\sigma(\gamma\gamma \rightarrow \pi^0\pi^0)$ vs \sqrt{s} , using phase shifts from the quark model (dashed line), from linear fits to the data (dotted line), and experimental data. The data are from Bienlein (*et al.*) (closed circles) [22], Marsiske *et al.* (open circles) [23], and Edwards *et al.* (closed triangles) [24]. The data have been corrected to full polar acceptance, $|\cos\theta| \leq 1.0$. (b) $\sigma(\gamma\gamma \rightarrow \pi^+\pi^-)$ vs \sqrt{s} with the same line labelling as (a). The curves have been corrected to have a limited polar acceptance to match the data: $|\cos\theta| \leq 0.6$. The data are from Behrend *et al.* (closed circles) [25], Boyer *et al.* (open circles) [26], and Aihara *et al.* (closed triangles) [27]. For additional comments see Figure 3.